1. Introduction

Distillation, also known as rectification, multistage or fractional distillation, is one of the most essential and widespread unit operations in the chemical process industry (Beneke et al., 2013; Billet, 1979; Fair, 2001; Kister, 1992; Mix et al., 1978; Moran, 2017; Stichlmair et al., 2021; Weiß, 1996). The underlying mechanism of distillation, separating a (binary) homogeneous liquid mixture based on its relative volatility, dates back to around 1200 BCE in ancient Mesopotamia where archaeological findings show simple distillation setups for perfume production (Levey, 1955). Detailed descriptions and illustrations of early distillation setups were presented by e.g. (Fairley, 1907; Kockmann, 2014). Throughout history, the best known application of a distillation process is presumably the alcohol enrichment of beverages. Distillation stills comparable to modern setups were developed in the early 19th century: A continuously operated distillation apparatus based on a vertical column was proposed in 1813. Mass transfer enhancing *column internals* like *packings* or *trays* were firstly used in 1820 and 1822, respectively (Kister, 1992).

Several generations of improved structured packings have been developed since the late 1950s, resulting in increased separation capacities and reduced costs which has led to the widespread application of structured packings in both absorption and distillation processes (Mendes, 2011; Spiegel and Meier, 2003). A mature understanding of the underlying mass and heat transfer phenomena as well as improved mass transfer correlations was developed in the last decades. According to (Schultes, 2013), the established models predict the separation performance for up to 90 % of the relevant industrial processes with an error margin of around 25 %, but deviations of up to 80 % are observed for the remaining applications. In the latter cases, column design needs to be supported with experimental separation performance investigations.

Such separation performance experiments are commonly carried out with standardized binary test mixtures under total reflux operating conditions and are widely discussed in the known literature. Despite its widespread use in industrial and academic settings, the conventional total reflux setup is not suitable for some specific use cases. As discussed by (Böcker and Ronge, 2005; Bradtmöller, 2017; Gutperl et al., 2022), it cannot be used for test mixtures with inert or non-volatile components which are, however, required to systematically investigate the separation of viscous mixtures with viscosities greater than $5 \ldots 6\,\mathrm{mPa\,s}$ at operating conditions (Böcker and Ronge, 2005; Bradtmöller, 2017; Bradtmöller and Scholl, 2016; Manivannan et al., 2019). Furthermore, total reflux conditions do not represent the conditions present in production columns which require product draws and are thus operated with finite reflux ratios.

This work, therefore, focuses on an alternative methodology suitable for separation perfor-

mance experiments with both finite and infinite reflux operating conditions. The developed plant setup is derived from the approach presented by (Böcker and Ronge, 2005) and is similar to a stripping column, inasmuch as product recycles are used to reduce the required amount of feedstock, and the feed inlet is located above the packed bed. After successful plant commissioning and characterization, the effect of reflux operating condition on separation performance was systematically investigated using the proposed experimental approach.

To support method development and experiment evaluation, relevant fundamentals of multistage distillation and separation performance measurements with total and partial reflux are summarized in chapter 2. As separation performance is commonly expressed in terms of the *height equivalent to a theoretical plate (HETP)* or the *height of a transfer unit (HTU)*, a link between both concepts is presented to point out the characteristics specific to each approach and to provide some background information addressing the question *Which measure should be preferred over the other?*. Furthermore, best practices and recommendations for designing and operating distillation plants for separation performance measurements are covered, since such information is required to ensure a robust plant design and operation. Use cases for which separation performance measurements at partial reflux are relevant are introduced in chapter 3 to not only highlight the necessity of such experiments, but also to derive the research hypotheses and objectives of this work. In addition, the developed plant concept, the corresponding plant setup and the experimental procedures used for the separation performance experiments, sample analyses and experiment evaluation are presented in detail. In particular, separation performance is evaluated in terms of HETP values, which are calculated based on the number of theoretical stages determined from *McCabe-Thiele stage constructions* and predicted with the *Delft mass transfer model*. Experimental and predicted results are compared to each other to address the applicability of the Delft model with respect to partial reflux experiments. A consistent propagation of relevant uncertainties allows assessing the robustness of the experimental results. Therefore, all calculation routines were implemented in and fully automated using the *Python* programming language. The results obtained from plant characterization and separation performance experiments with total and partial reflux operating conditions are discussed in chapter 4. As partial reflux experiments are commonly considered less sound than total reflux experiments, special attention is paid to the uncertainty components related to the reflux condition. Furthermore, the proposed plant concept, experimental setup and corresponding experimental procedures are evaluated based on the obtained experimental results to not only identify potential improvements increasing the applicability and usability of the presented methodology, but also highlight future research activities enabled by separation performance measurements with partial reflux.

2. Theoretical Background and Literature Review

2.1. Distillation and Separation Fundamentals

2.1.1. Equilibrium Thermodynamics

Mixture separation of binary mixtures is primarily based on the differing *distribution coefficients* K_i of each mixture component (Sorensen, 2014). The distribution coefficient, also abbreviated as the *K-value*, of a given mixture component i depends on both temperature and pressure and is defined as (Kister, 1992; Sorensen, 2014):

$$K_i = \frac{\text{molar fraction of component } i \text{ in vapor phase}}{\text{molar fraction of component } i \text{ in liquid phase}} = \frac{y_i}{x_i} \tag{2.1}$$

A high K-value indicates a high volatility, or tendency of the component to vaporize and accumulate in the vapor phase, whereas less volatile components show lower K-values. For a binary mixture containing components 1 and 2, its relative volatility α_{12} is defined as (Kister, 1992):

$$\alpha_{12} = \frac{K_1}{K_2} = \frac{y_1 \cdot x_1^{-1}}{y_2 \cdot x_2^{-1}} = \frac{y_1 \cdot x_2}{y_2 \cdot x_1} = \frac{y_1 \cdot (1 - x_1)}{x_1 \cdot (1 - y_1)} \tag{2.2}$$

Equation (2.2) can be rearranged to express the *vapor-liquid-equilibrium (VLE)*, so that y_1 is calculated in terms of x_1 and α_{12} (Kister, 1992; Sorensen, 2014):

$$y_1 = \frac{\alpha_{12} \cdot x_1}{1 + (\alpha_{12} - 1) \cdot x_1} \tag{2.3}$$

This expression is often used in conjunction with *xy-diagrams*, which are also known as *equilibrium diagrams* and are especially relevant for *McCabe-Thiele stage constructions*, see section 2.2.1.2. As shown in figure 2.1, higher relative volatilities result in more convex equilibrium curves with higher molar fractions present in the vapor phase than lower relative volatilities. Therefore, binary mixtures with a high relative volatility require less separation effort to obtain pure components than binary mixtures with low volatility (Kister, 1992).

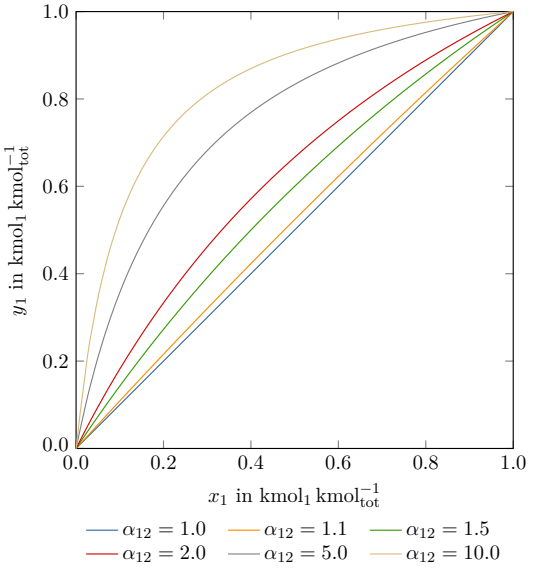

Figure 2.1.: Equilibrium curve in dependence of relative volatility α_{12}, calculated according to equation (2.3)

However, for most mixtures, the relative volatility α_{12} varies with mixture composition and temperature. To describe this behavior, different approximations have been established; a detailed discussion can be found in e.g. (Kister, 1992). A simple approximation is based on the geometrically averaged relative volatility $\overline{\alpha}_{12}$ as given in equation (2.4) (King, 1980). $\alpha_{12,\mathrm{I}}$ and $\alpha_{12,\mathrm{II}}$ represent the relative volatilities at minimum as well as maximum mixture composition and an arithmetically averaged mixture temperature (King, 1980).

$$\overline{\alpha}_{12} = \sqrt{\alpha_{12,\mathrm{I}} \cdot \alpha_{12,\mathrm{II}}} \tag{2.4}$$

The liquid phase is generally described by *Raoult's law* which defines a relation between the partial pressure p_i of component i, its vapor pressure p_i^0 and its molar fraction x_i. Deviations from ideal behavior ($\gamma_i = 1$) are described by the activity coefficient γ_i which is a function of temperature T and liquid phase composition x_i (Kleiber, 2020; Sorensen, 2014):

$$p_i = x_i \cdot p_i^0 \cdot \gamma_i(T, x_i) \tag{2.5}$$

For the vapor phase, *Dalton's law* provides a relation between partial pressure p_i, molar fraction in vapor phase y_i and the total pressure p_{tot}:

$$p_i = y_i \cdot p_{\mathrm{tot}} \tag{2.6}$$

Similar to activity coefficients, nonidealities of the vapor phase can be expressed by fugacity coefficients φ_i. According to (Sorensen, 2014) nonidealities become relevant at elevated operating pressures of $p \geq 7 \ldots 10\,\mathrm{bar(a)}$. Since all experiments presented in this work were conducted with $p = 100\,\mathrm{mbar(a)}$ an ideal vapor phase can be assumed, and thus fugacity coefficients are not considered.

Inserting equations (2.5) and (2.6) into equation (2.2) expresses the relative volatility as a function of activity coefficients γ_i and vapor pressures p_i^0 (Kister, 1992; Sorensen, 2014):

$$\alpha_{12} = \frac{\gamma_1(T, x_1) \cdot p_1^0}{\gamma_2(T, x_2) \cdot p_2^0} \tag{2.7}$$

The activity coefficients needed to describe nonideal mixture behavior are commonly estimated by using either g^E *models* or *equations of state (EoS)*[1].

g^E models are based on the relation between the excess Gibbs energy g^E and activity coefficient γ_i (Gmehling and Kleiber, 2014):

$$g^\mathrm{E} = \sum_i x_i \cdot g_i^\mathrm{E} = R\,T \sum_i x_i \cdot \ln \gamma_i \Longleftrightarrow \ln \gamma_i = \frac{g_i^\mathrm{E}}{R\,T} \tag{2.8}$$

For a pure liquid, the excess Gibbs energy g^E needs to satisfy the following condition (Gmehling et al., 2019):

$$g^\mathrm{E}(x_i = 1) \to 0. \tag{2.9}$$

For a binary liquid mixture with components 1 and 2, the *Porter equation* given in equation (2.10) fulfills this requirement. It is often considered as the simplest *activity coefficient model*, because it contains only a single model parameter A:

$$\frac{g^\mathrm{E}}{R\,T} = A\,x_1\,x_2 \tag{2.10}$$

Due to its simplicity, the Porter equation can only be applied to a very limited number of nonideal liquid mixtures, and thus more versatile approaches are required (Gmehling et al., 2019). A general algebraic approach to describe nonideal binary mixtures using series expansion was proposed by (Redlich and Kister, 1948a):

$$\frac{g^\mathrm{E}}{R\,T} = x_1\,x_2\,\left[A + B\,(x_1 - x_2) + C\,(x_1 - x_2)^2 + \ldots\right] \tag{2.11}$$

Despite the versatility of equation (2.11), this approach is only applicable to binary mixtures and the influence of temperature on the activity coefficient is neglected (Gmehling et al., 2019). Therefore, improved activity coefficient models, such as the *Wilson equation* (Wilson, 1964), the

[1] EoS are not in scope of this work, and thus not elaborated further. Refer to e.g. (Gmehling and Kleiber, 2014; Gmehling et al., 2019; Kleiber, 2020; Stichlmair et al., 2021) for details on EoS.

NRTL model (Non-random two-liquid model) (Renon and Prausnitz, 1968) and the *UNIQUAC approach (universal quasichemical)* (Abrams and Prausnitz, 1975), are commonly used today. These models contain additional parameters which consider local concentrations around mixture molecules and allow for an improved description of mixture nonidealities.

2.1.2. Continuous Distillation

Continuous multistage distillation operates under countercurrent flow conditions and can be illustrated as a cascade of multiple *equilibrium stages*, see figure 2.2 (Vogelpohl, 2021).

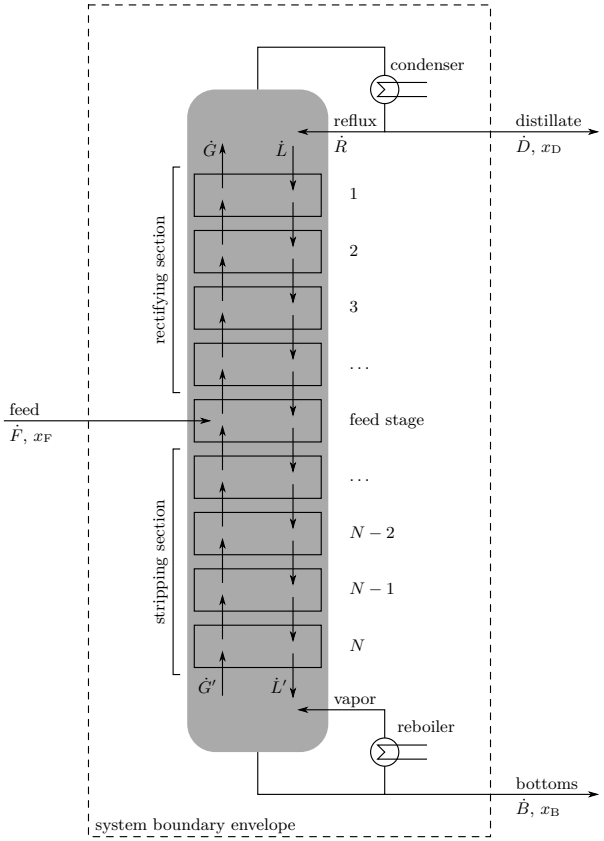

Figure 2.2.: Multistage distillation represented as a cascade of equilibrium stages, based on (Kister, 1992; Sorensen, 2014; Stichlmair et al., 2021; Vogelpohl, 2021)

According to (Kister, 1992), each equilibrium stage operates in steady state resulting in

constant vapor and liquid output streams. Since input streams are assumed being perfectly mixed after entering the stage, equilibrium between the vapor and liquid output streams is achieved instantaneously (Kister, 1992). The separation is accomplished by feeding vapor from the reboiler to the bottom stage[2] N. As liquid from stage N comes into contact with the vapor, partial condensation occurs. As a result, some liquid is vaporized due to the released heat of condensation, whereby volatile mixture components are enriched in the vapor. This condensation and vaporization continues throughout every stage, resulting in a purified vapor stream leaving the top stage. The overhead vapor is then (partially) condensed and either drawn from the system as the *distillate* or returned to the top stage as the *reflux*. Since the reflux trickles down inside the column, it also provides liquid in each stage. Liquid leaving the bottom stage is either drawn from the system as the *bottom product*, also referred to as *bottoms*, or returned to the reboiler.

Using the system boundary drawn in figure 2.2 and assuming a steady-state operation, such that there is no accumulation inside the system boundary, the *molar balance of a continuous distillation* can be written as:

$$\dot{F} = \dot{D} + \dot{B} \tag{2.12}$$

Furthermore, the *reflux ratio* ν is defined based on the molar flow of reflux $\dot{R}$ and distillate $\dot{D}$ as shown in equation (2.13) (Kister, 1992; Sorensen, 2014). For a boiling liquid reflux, the reflux ratio can also be expressed with the internal liquid stream $\dot{L}$, since $\dot{R} = \dot{L}$ (Schönbucher, 2002):

$$\nu = \frac{\dot{R}}{\dot{D}} = \frac{\dot{L}}{\dot{D}} \tag{2.13}$$

Equation (2.13) is also referred to as the *external reflux ratio* and takes values of $\nu > 0$ (Sorensen, 2014). Alternatively, the *internal reflux ratio* ν_{int} with values of $0 \leq \nu_{\text{int}} \leq 1$ is described as (Sorensen, 2014):

$$\nu_{\text{int}} = \frac{\dot{L}}{\dot{G}} \tag{2.14}$$

Similarly, the *reboil ratio* ν', also known as the *stripping ratio*, is given based on the molar flow of vapor $\dot{G}'$ and the bottoms $\dot{B}$ (Kister, 1992; Sorensen, 2014):

$$\nu' = \frac{\dot{G}'}{\dot{B}} \tag{2.15}$$

[2]Throughout this work, stages are numbered from top to bottom (stage 1 at the top and stage N at the bottom of the column) which is in accordance with e.g. (Kister, 1992; McCabe and Thiele, 1925; Sorensen, 2014). However, numbering from bottom to top is also possible and can be found in e.g. (Kleiber, 2020; Stichlmair et al., 2021). Furthermore, indices referring to a stage number indicate the stage where the designated flow originates. For example, $\dot{L}_4$ denotes the molar liquid flow leaving stage 4 and entering stage 5, whereas $\dot{G}_4$ is the molar vapor flow from stage 4 into stage 3.

Special attention should be focused on the feed stage. As shown in figure 2.2, stages above the feed stage are called the *rectifying section*, while stages below the feed stage belong to the *stripping section*. Furthermore, internal molar vapor flows $\dot{G}'$ and $\dot{G}$ as well as liquid flows $\dot{L}'$ and $\dot{L}$ depend on the *feed condition* q, which results in $\dot{G}' \neq \dot{G}$ or $\dot{L}' \neq \dot{L}$ for most cases. The feed condition is defined by the molar enthalpy at the bubble point h'_{F}, the molar enthalpy as saturated vapor h''_{F}, the molar enthalpy at feed condition h_{F} and the molar enthalpy of vaporization $\Delta h_{\mathrm{vap,F}}$ (Billet, 1979):

$$q = 1 + \frac{h'_{\mathrm{F}} - h_{\mathrm{F}}}{\Delta h_{\mathrm{vap,F}}} = 1 + \frac{h'_{\mathrm{F}} - h_{\mathrm{F}}}{h''_{\mathrm{F}} - h'_{\mathrm{F}}} \tag{2.16}$$

General trends for the resulting flows of vapor $\dot{G}'$ and $\dot{G}$ as well as liquid $\dot{L}'$ and $\dot{L}$ are summarized in table 2.1.

Table 2.1.: Feed conditions, based on (Billet, 1979; Sorensen, 2014; Stichlmair et al., 2021)

feed condition	h_{F}	q	vapor streams	liquid streams
subcooled liquid	$h_{\mathrm{F}} < h'_{\mathrm{F}}$	$q > 1$	$\dot{G}' > \dot{G}$	$\dot{L}' > \dot{L}$
boiling liquid	$h_{\mathrm{F}} = h'_{\mathrm{F}}$	$q = 1$	$\dot{G}' = \dot{G}$	$\dot{L}' > \dot{L}$
wet vapor	$h'_{\mathrm{F}} < h_{\mathrm{F}} < h''_{\mathrm{F}}$	$0 < q < 1$	$\dot{G}' < \dot{G}$	$\dot{L}' > \dot{L}$
saturated vapor	$h_{\mathrm{F}} = h''_{\mathrm{F}}$	$q = 0$	$\dot{G}' < \dot{G}$	$\dot{L}' = \dot{L}$
superheated vapor	$h_{\mathrm{F}} > h''_{\mathrm{F}}$	$q < 0$	$\dot{G}' < \dot{G}$	$\dot{L}' < \dot{L}$

2.1.3. Multistage Distillation Apparatus

Multistage distillation is commonly performed in *distillation columns*. Since instantaneous equilibrium can only be reached in theory, phase contact between vapor and liquid streams inside the column needs to be intensified for which different types of *mass transfer equipment*, *column internals* and accessory devices were developed in the past. While *trays*, *unstructured packings* and *structured packings* are the most common types of mass transfer equipment used for multistage distillation, this work focuses on structured packings only. Equipment design and selection varies based on several factors such as feedstock properties, product specification, operating conditions and process complexity, process efficiency, capacity and throughput, capital expenses and operating costs as well as in-house expertise (Kister, 1992; Olujić, 2014). Detailed discussions and comparisons of widely used mass transfer equipment as well as column internals and accessories can be found in e.g. (Billet, 1979; Billet, 1995; Górak and Olujić, 2014; Kister, 1992).

To ensure efficient column operation with respect to its capacity and an optimal mixture separation, the *gas load* $u_{\mathrm{G,s}}$ and *liquid load* w_{L} need to be considered. The gas load is defined as a superficial gas velocity $u_{\mathrm{G,s}}$, and thus based on the volumetric vapor or gas flow rate $\dot{V}_{\mathrm{G}}$

and the cross-sectional area of the (unpacked) column A_{col}:

$$u_{\mathrm{G,s}} = \frac{\dot{V}_{\mathrm{G}}}{A_{\mathrm{col}}} \tag{2.17}$$

Alternatively, gas load can be expressed in terms of the f-factor f_{G} based on superficial gas velocity $u_{\mathrm{G,s}}$ and gas density ρ_{G}:

$$f_{\mathrm{G}} = u_{\mathrm{G,s}} \cdot \rho_{\mathrm{G}}^{0.5} \tag{2.18}$$

Similar to equation (2.17), the liquid load w_{L} is defined using the volumetric liquid flow rate $\dot{V}_{\mathrm{L}}$:

$$w_{\mathrm{L}} = \frac{\dot{V}_{\mathrm{L}}}{A_{\mathrm{col}}} \tag{2.19}$$

These loads depend on the column configuration and operation, and thus can vary along the column height. In such cases, representative column sections should be considered. The valid operating range for a given type of structured packings can be described based on the *load diagram* (Kleiber, 2020):

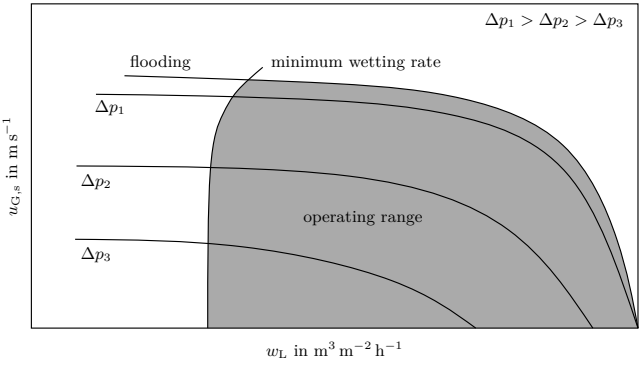

Figure 2.3.: Load diagram for structured packings, based on (Kleiber, 2020; Molzahn and Schmidt, 1975; Stichlmair et al., 2021)

The lower limit of the operating region is defined by the *minimum liquid load* (Kleiber, 2020; Sattler, 2001) or *minimum wetting rate (MWR)* where the packing surface is not wetted sufficiently and *underwetting* occurs (Kister, 1992). This results in a small effective mass transfer area, and thus a poor separation efficiency. In contrast, at high liquid or gas loads, entrainment increases successively, resulting in *flooding* or *phase inversion* which is considered the upper boundary of the operating region (Billet, 1995; Kister, 1992; Sattler, 2001).

Depending on liquid load w_{L} and gas load $u_{\mathrm{G,s}}$, the following operating regimes can commonly

be identified for structured packings (Kister, 1992):

- Turndown maldistribution regime: At low column load, separation efficiency is reduced due to the turndown limit of the packing and/or the liquid distributor. If proper liquid distribution is ensured, the upper boundary of this region represents the MWR of the packing.
- Preloading regime: Separation efficiency is constant and independent of column load due to a turbulent liquid film, good surface wetting and a good mass transfer. Most columns are designed to operate within this region.
- Loading regime: The column transitions from normal to flooded operation. As the liquid holdup increases, the separation efficiency reaches its maximum and drops thereafter due to large entrainment. Even though maximum efficiency can be achieved in this region, it is not commonly used in column design due to its proximity to the flood point.
- Flooding regime: Instable column operation and poor efficiency occur due to heavy entrainment and flooding. Therefore, this region is avoided.

The achieved separation efficiency is related to the fluiddynamic conditions inside the packed bed (Kister, 1992): With higher column loads, the effective interfacial area increases, and thus mass transfer is enhanced, which improves efficiency. In contrast, an increased vapor load decreases the residence time of the vapor phase, which in turn results in a decreased efficiency. Since both effects are balanced for most corrugated-sheet packings, the overall efficiency is widely independent of both the vapor and liquid loads, resulting in a constant separation efficiency in the preloading regime. For some packings, however, a sloped relation between column load and separation efficiency is observed as the decrease in vapor phase residence time can dominate the increasing effect of enhanced mass transfer, resulting in an overall reduced efficiency. Different types of packings, characteristic operating points and operating regimes as well as their corresponding graphical representation in the *efficiency diagram* are discussed by (Kister, 1992).

Proper column design and packing selection are vital for reliable plant operation and mixture separation. This is especially true for demanding separation tasks where low specific pressure drops or high turndown ratios with wide operating ranges are needed. To satisfy these requirements, several generations of structured packings have been developed (Meier et al., 1979; Spiegel and Duss, 2014; Spiegel and Meier, 2003). As further improvements in packing performance seem to be limited by conventional manufacturing processes, additive manufacturing is currently evaluated to realize enhanced packing geometries with improved capabilities; see e.g. (Ashour et al., 2022; Dejean et al., 2020; Neukäufer et al., 2022; Neukäufer et al., 2021; Sarajlic et al., 2022).

Furthermore, improved or alternative distillation apparatuses are the subject of current research activities which focus on process intensification, e.g. wetted wall columns (Reitze et al.,